Climate Dynamics (2003) 20: 689–703
DOI 10.1007/s00382-002-0299-8

B.G. Hunt · T.I. Elliott

Secular variability of ENSO events in a 1000-year climatic simulation

Received: 10 October 2001 / Accepted: 4 November 2002 / Published online: 4 March 2003

Abstract The CSIRO Mark 2 coupled global climatic model has been used to generate 1000 years of simulated climatic variability corresponding to present climatic conditions. A small climatic drift was noted during the simulation, and all results presented are based on detrended conditions. The emphasis here is on El Niño/Southern Oscillation (ENSO) events and their secular variability during the simulation. A number of features of the simulated ENSO climatology are presented and compared with observations. These demonstrate that the model reproduced the major characteristics of observed ENSO variability. A variety of analyses is given to illustrate secular variability of ENSO-related climate. Thus, while the simulated Southern Oscillation is shown to be a robust feature of the model climatology, decadal and oscillatory time variations occurred. Time-smoothing of the Southern Oscillation Index revealed underlying multi-decadal episodes, with associated climatic anomalies. Examination of 'strong' ENSO events highlighted an asymmetry between El Niño and La Niña events, similar to that observed, with clear secular variability in the occurrence rate of La Niña events. Persistent (multi-annual) ENSO events, such as occurred in the 1990s, were found to exist within the simulation, suggesting that these may be attributable to natural climatic variability. An investigation of the temporal variation of the anomalous depth of the 20 °C isotherm in the Pacific Ocean, revealed secular variability, which, if predictable, could identify decadal-length climatic trends. Other analyses involved the behaviour of the Pacific North American Oscillation and its secular variability. Distinct climatic impacts over North America were identified with this variability. Importantly, the simulation identified a number of features of ENSO-related climatic variability which have been poorly, if at all, documented in observations to date.

B.G. Hunt (✉) · T.I. Elliott
CSIRO Atmospheric Research, PMB1,
Aspendale, Victoria 3195, Australia
E-mail: barrie.hunt@csiro.au

1 Introduction

El Niño/Southern Oscillation events constitute the largest source of interannual climatic variability. Despite the importance of such events, the brevity of the directly observed record (about 120 years, Allan et al. 1996) limits our knowledge of their secular variability. As a consequence, it remains a matter of dispute whether, for example, the multiple El Niño events of the early 1990s are attributable to the greenhouse effect (Trenberth and Hoar 1996), or are just a consequence of natural climatic variability (Allan and D'Arrigo 1999).

The actual situation is rather more complex and subtle than implied already. As noted by Lui and Huang (2000) there is an observed warming trend in the low-latitude Pacific Ocean, which, however caused, may be generating an oceanic state more conducive to El Niño events. This warming trend is associated with, and feeds back upon, a weakening of the zonal wind stress in this region.

Other important questions concerning ENSO characteristics also exist. These include the frequency of 'super' ENSO events (such as the 1982/3 El Niño), the interaction between ENSO events and the Interdecadal Pacific Oscillation, relative frequency of El Niño versus La Niña events, the stationarity of ENSO climatology, variations in teleconnections, spatial characteristics, oceanic responses, etc. Not all of these will be discussed here.

While knowledge of ENSO events extends back some centuries, see for example Quinn et al. (1987), this is based on a variety of proxy sources or historical data, and substantial questions arise concerning the consistency of these sources (Allan and D'Arrigo 1999). In addition, there are concerns about future ENSO

behaviour, specifically whether ENSO characteristics will alter under enhanced greenhouse conditions. Thus Timmermann et al. (1999) and Wilson and Hunt (1997) found an increase in the frequency of El Niño events in their simulations, while Knutson et al. (1997) did not.

The answer to the last question can be attempted via simulations with coupled global climatic models (GCMs). Hence, it is important, for this reason alone, to evaluate the ability of models to replicate the behaviour of ENSO events for the present climate in order to have confidence in any simulations of greenhouse-induced ENSO changes. In addition, a sound knowledge of the secular variability of simulated events is necessary in order to differentiate between natural climatic variability and greenhouse-induced climatic changes in ENSO (Knutson and Manabe 1994).

Many previous studies of the secular variability of ENSO have been primarily restricted to investigations of sea surface temperature (SST) behaviour, see for example Wang and Ropelewski (1995), Chao et al. (2000) and Zhang et al. (1998). More broadly based studies of ENSO events have been provided in reviews such as that edited by Diaz and Markgraf (1992).

The aims of the present study are:

1. To document the ability of the CSIRO Mark 2 model to simulate the basic characteristics of ENSO events, thus establishing its credibility in the subsequent study of secular variability of ENSO
2. To illustrate, by a range of examples, the secular variability of ENSO events and their related atmospheric and oceanic perturbations
3. To explain, where possible, the causes or mechanisms responsible for this secular variability
4. Finally, to present examples of the climatic *impacts* of the secular variability.

2 Model ENSO climatology

The model used here is the CSIRO Mark 2 coupled global climatic model. Various aspects of the model's overall climatology have been presented in a number of papers (Gordon and O'Farrell 1997; Hirst et al. 2000; Watterson et al. 1995; Hunt 2001). In particular, a number of ENSO characteristics of the present model and 16 other coupled models have been documented by AchutaRao and Sperber (2000). This documentation highlights the difficulties all of these models have in reproducing adequately the observed ENSO climatology. The principal deficiencies of the CSIRO model revealed in this documentation are low-latitude Pacific Ocean SST anomalies, which are too weak by a factor of about two, resulting in rainfall anomalies which are also too small, and an ENSO periodicity greater than the observed range of two to seven years. Overall, the CSIRO model appeared to be a mid-level performer in this intercomparison. However, this model performed well in the more extensive intercomparison presented by Covey et al. (2000).

The present analysis is based on a 1000-year simulation which was an extension of the 100-year run used in the earlier two intercomparisons. The model experienced a slight downwards drift in the annual mean, globally averaged screen air temperature, from approximately 13.8° to 13.6° during the course of the 1000-year simulation. There was a corresponding drift in other climatic variables. Consequently, all results presented here have been detrended by removing the drift at each gridpoint prior to analysis.

A number of analyses are presented here to document further the ability of the CSIRO Mark 2 coupled model to reproduce critical features of the observed ENSO climatology.

Figure 1 compares observed (NCEP/NCAR reanalysis for 1949 to 1990) and simulated composited El Nino SST anomalies for December, January and February. The corresponding comparison for La Nina events is shown in Fig. 2. For consistency with the model, all NCEP/NCAR observations presented here have been interpolated to R21 resolution from their original resolutions. The model replicated the observed features extremely well, not only in the Pacific Ocean but also the Atlantic and Indian oceans. The characteristic equatorial maximum in the value of the SST anomalies in the Pacific Ocean, and the horseshoe pattern of opposite sign anomalies, together with the reversal of signs between El Niño and La Niña events, which are critical features of ENSO events, are all simulated. The major discrepancy, as noted, is that the model simulation does not attain the observed amplitude of the SST anomalies in the equatorial Pacific Ocean, and the simulated maxima are too far to the west. These outcomes are attributable to various model deficiencies, especially the low horizontal resolution.

A basic ENSO characteristic is illustrated in Fig. 3, where the NINO3 (5°S to 5°N, 150°W to 90°W) SST is correlated with the global SST for all 1000 years of the simulation, together with corresponding results for the NCEP/NCAR reanalysis. All the observed characteristics are replicated by the model. Figure 4 shows a similar comparison for NINO3 SST and oceanic rainfall. The model, not surprisingly, performs less well here, with too extensive an area of positive correlation over the Pacific Ocean and maximum correlation too far to the west. The latter feature is a

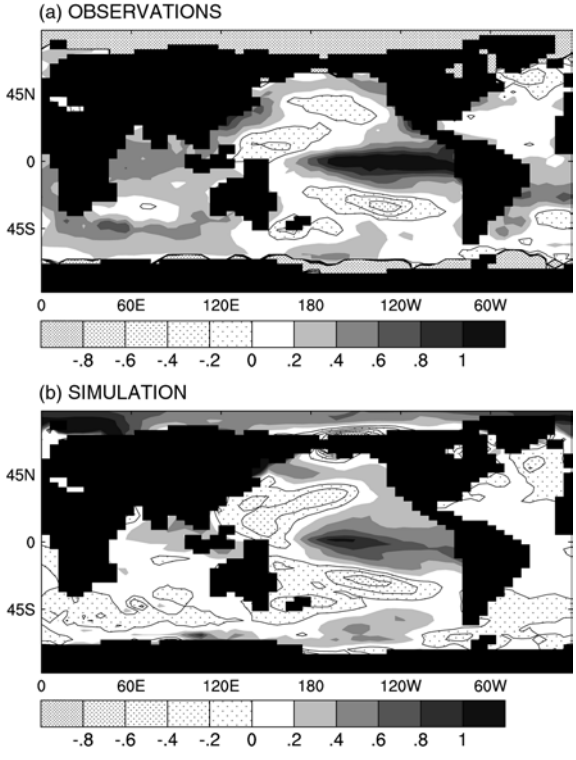

Fig. 1a, b Composite of December, January and February SST anomalies for El Niño events; *top*, observations based on NCEP/NCAR reanalysis for 1949 to 1990; *bottom*, 1000-year simulation. The *shading bar* is in °C

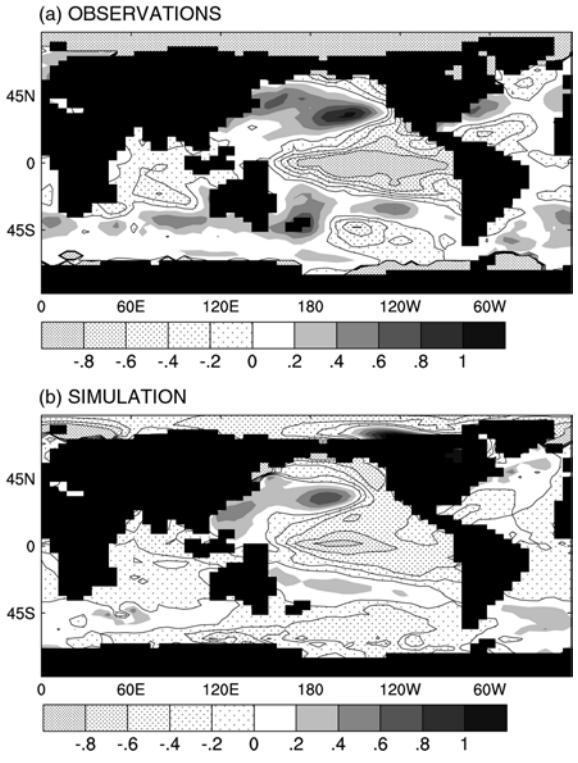

Fig. 2a, b As for Fig. 1 but for La Niña events

consequence of the displacement of the maximum SST to the west in the simulation, as noted already. Nevertheless, the basic observed features are replicated by the model.

The observed correlation in Fig. 4 when based on the original T42 horizontal resolution of the NCEP/NCAR reanalysis was much weaker and lacked a clear ENSO signal, as well as being dominated by small-scale features.

The simulated correlation in Fig. 4 was also computed for a number of 41-year periods, as opposed to using all 1000-years of the simulation, to investigate whether a sampling problem existed given that only 41 years were available for the NCEP/NCAR reanalysis. The simulated pattern of Fig. 4 was reproduced in each of these samples, but all exhibited more small-scale noise, which tended to improve the agreement with observation.

An indication of the temporal variability of ENSO in the simulation using montly-mean values is provided in Fig. 5. This figure compares the Southern Oscillation Index (SOI) with SST anomalies for the NINO3.4 region (5°S to 5°N, 170°W to 120°W) for a 100-year period of the simulation. The observed anti-correlation (see a typical Climate Diagnostics Bulletin of NOAA, web address http://www.cpc.ncep.noaa.gov) is well simulated, with the negative SOI values of El Niño events being associated with positive temperature anomalies. The correlation coefficient for the 1000-year period was –0.45, having extremely high significance given the length of the simulation. The corresponding correlation coefficient for the 41 years of the NCEP/NCAR data set was –0.50. The small amplitude of the temperature anomalies is readily apparent in this figure. A detailed examination of NINO3.4 surface temperature anomalies, not shown, revealed that ENSO events in the model were phase-locked to the seasonal cycle, with peaks occurring in the December–January period.

A recent analysis of the processes governing the ENSO cycle in the present 1000-year simulation has shown that the delayed oscillator mechanism prevailed (Vimont et al. 2002). No further analysis of this mechanism has been made here.

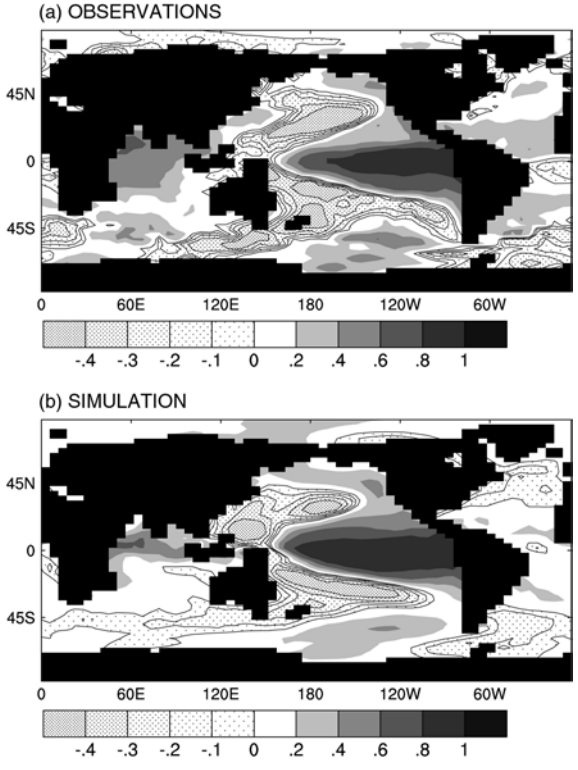

Fig. 3a, b Correlation of the NIÑO3 SST with the global SST: *top*, observations based on NCEP/NCAR reanalysis for 1949 to 1990; *bottom*, 1000-year simulation

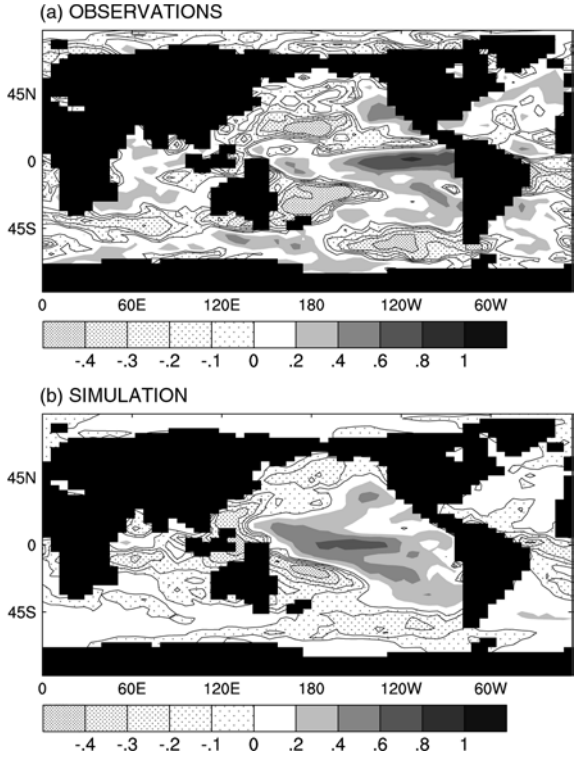

Fig. 4a, b As for Fig. 3 but NIÑO3 SST correlation with oceanic rainfall

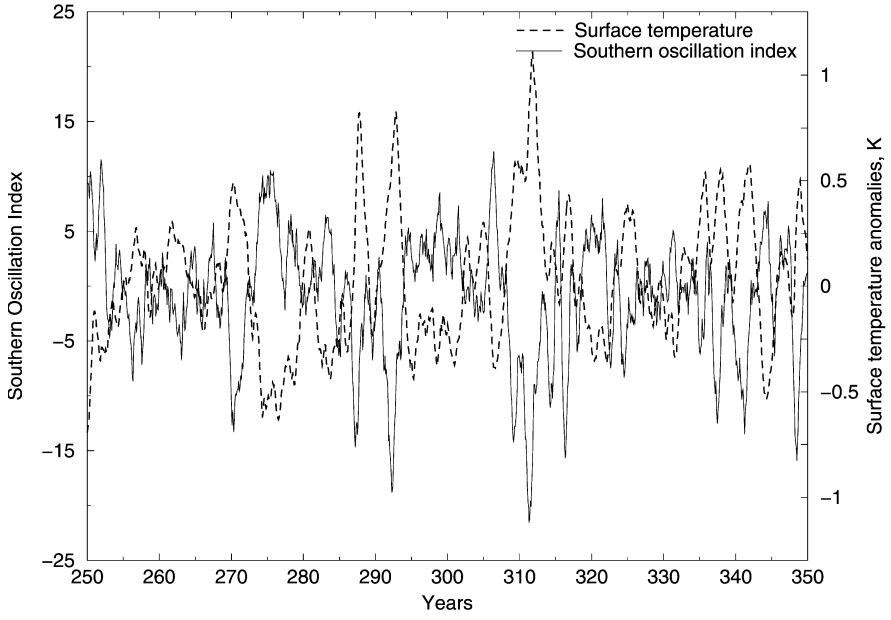

Fig. 5 Comparison of the Southern Oscillation Index and the SST for the NIÑO3.4 region for a 100-year period of the simulation. Monthly mean values are shown

Prior to considering the secular variability of ENSO events a check was made concerning the stationarity of the climate within the 1000-year simulation. This was investigated by generating time series of surface temperature and rainfall for a number of geographical regions. A representative sample is given in Fig. 6. This illustrates the surface temperature for the NINO3.4 region for all 1000 years of the simulation. The dominant feature of the time series is the interannual variability, upon which are superimposed decadal fluctuations. A temperature range of 2 °C was associated with this variability. Two particularly noticeable temperature fluctuations indicative of secular variability occurred in the time series, around years 400 and 750, but these were only of about 20 years duration. There are no distinct signs of long-term trends, changes in regime state or other marks of non-stationarity. Similar time series were obtained for other regions and also for rainfall time series.

Thus, the investigation of secular variability of ENSO events presented here is based on a stationary climatic state. In this regard, the comment by Diaz and Pulwarty (1994) is relevant, namely: "*it appears that ENSO may have operated in a substantially similar fashion over the past thousand years as it has during the past century*." This implies that if the model had simulated a non-stationary state then this would indicate either some unknown climatic phenomenon had been activated, or, more likely, a model error.

In summary, the model has been shown to replicate most of the climatological features of observed ENSO events, suggesting that it should also be able to capture secular variability of such events as induced by internal climatic variability, as well as providing confidence for the use of the model in greenhouse simulations (Gordon and O'Farrell 1997) and multi-seasonal predictions (Hunt 2000a).

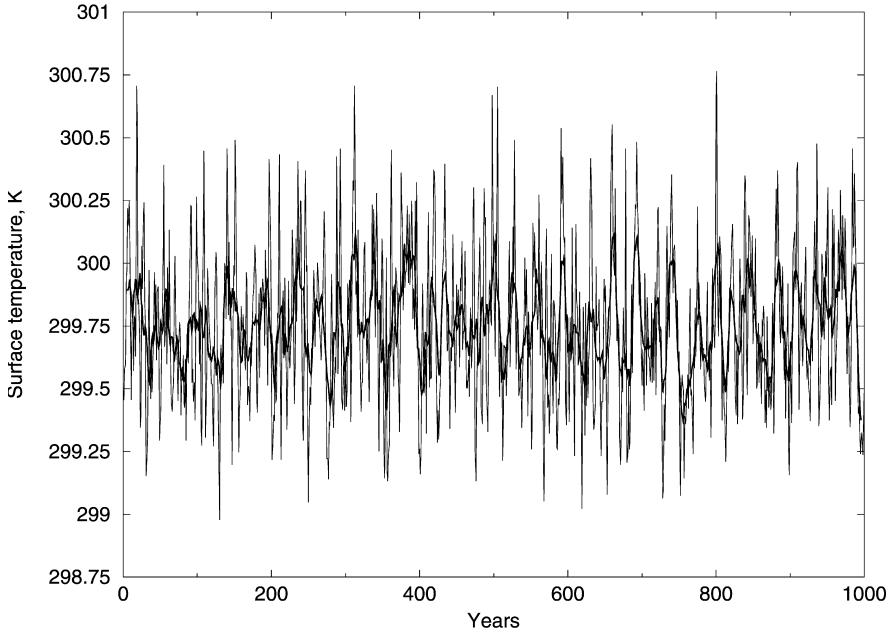

Fig. 6 Surface temperature for the NINO3.4 region for all 1000 years of the simulation. Annual mean values are shown with a superimposed curve based on a 10-year running mean

3 Secular characteristics

The secular variability of ENSO-related events within the 1000-year simulation will be illustrated by a number of individual analyses.

3.1 The southern oscillation index

This index is probably the most commonly accepted indicator of ENSO activity. Figure 7 presents the SOI value for all 1000 years of the simulation using monthly mean outputs. These values are very similar to the corresponding observations from 1876 to 1998 (Allan 2000) and also to an alternative seasonal SOI chronology dating back to 1600 AD derived by Lough (1992) from tree ring samples from arid sites in western North America.

An examination of Fig. 7 reveals the following basic features:

1. The overall stability of the index.
2. There are no *sustained* period of abnormally high or low index values. Decadal length periods of low activity occur near years 110, 540 etc.
3. Sequences of years with persistent El Niño (years 310, 690 etc.) or La Niña (years 355, 570 etc.) can be identified.
4. Outliers occur quite frequently, but are more apparent for El Niño rather than La Niña events.

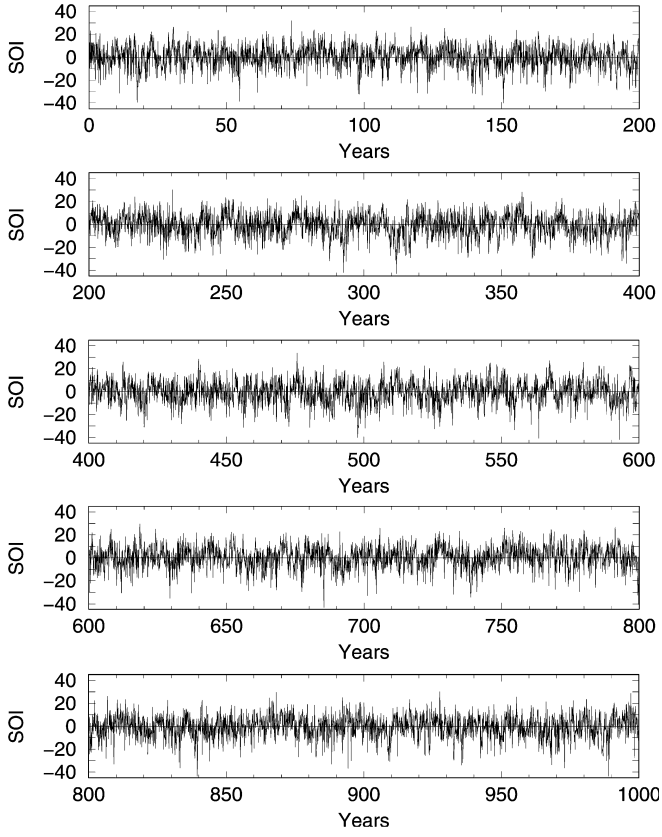

Fig. 7 Time series of the SOI using monthly values for all 1000 years of the simulation

Given the short duration of the observed SOI record (Allan 2000), not all the features shown in Fig. 7 have been recorded, for example, the decadal length trends (years 410, 570 etc.), hence this figure may indicate possible future outcomes.

Examination of the standard deviation of the simulated SOI time series using a 50-year sliding window (not shown) revealed variations of only 10% between minimum and maximum values. The result also confirms the stationarity of the model climate. In general, perturbations in the SOI standard deviation could be identified with SST anomalies in the tropical Pacific Ocean.

However, when a time series plot of SOI amplitudes greater than |25| was examined, see Fig. 8, more distinctive behaviour resulted. The value of |25| was chosen as it represents an ENSO event of sufficient magnitude to initiate climatic impacts. The figure highlights the relative preponderance of El Niño versus La Niña events of this magnitude in the simulation. A similar outcome is also apparent in the limited observations, from Allan et al. (1996), shown in Fig. 8. The preference for strong El Niño SOI values is consistent with the relative frequency of occurrence of large amplitude positive SST anomalies in the tropical Pacific Ocean, see Fig. 9.

While close examination of Fig. 7 suggests that some of the individual, extreme SOI values in Fig. 8 may represent random responses, most of these values are components of distinct El Niño or La Niña events. The La Niña events in Fig. 8 indicate strong signs of secular variability. For example, relatively few major La Niña events occurred in the first 400 years of the simulation,

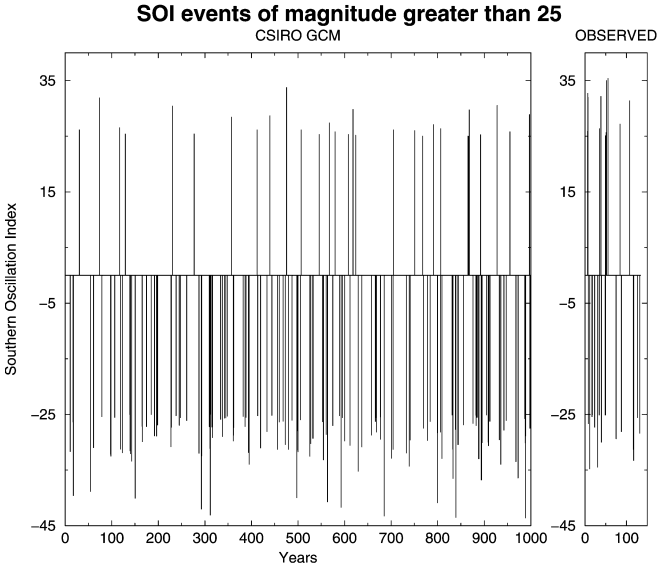

Fig. 8 Plot of SOI values with magnitudes greater than 25 as simulated in the 1000-year run is shown in the *left hand panel*, observations in the *right hand panel*. Monthly data were used, hence multiple values exist for some years

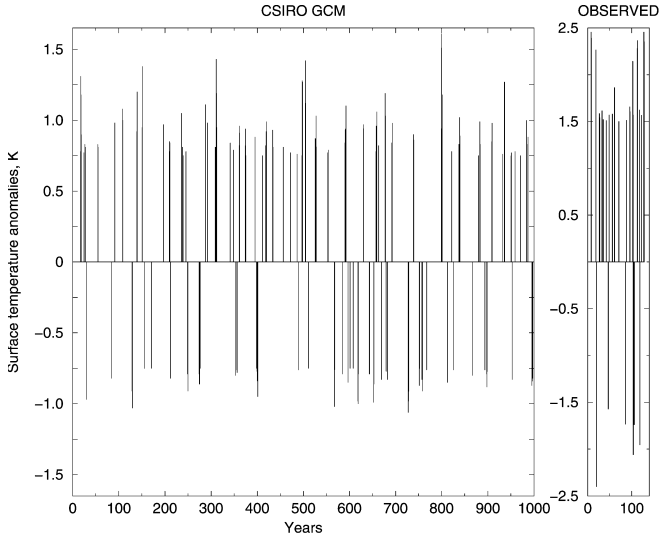

Fig. 9 Plots of surface temperature anomalies for the NINO3.4 region having magnitudes greater than 0.75 K for the simulation and 1.5 K for observations are shown in the *left and right hand panels* respectively. Monthly data were used hence multiple values exist for some years

with at least one period of 100 years without such an event. Subsequently, the frequency of La Niñas increased up to about year 620, when another period of almost 100 years duration occurred without a major La Niña event. It needs to be emphasised that the lack of major La Niña events does not mean that extensive negative SST anomalies did not occur in the tropical Pacific Ocean, but only that the amplitude of such anomalies was too small to excite a significant SOI pulsation.

In contrast, strong El Niño events occurred frequently and consistently in the simulation according to Fig. 8. While there are several periods of about 20 years without such strong events, overall the impression from the figure is that they are a characteristic feature of the simulated climate, and that on several occasions multi-annual events occurred.

In terms of secular variability, Fig. 9 highlights the intermittency of large amplitude SST anomalies in the low-latitude Pacific Ocean which are associated with strong ENSO events. Results for both the simulation and observations, from Folland and Rowell (1995), are compared in the figure. The criterion used to select the minimum value of SST anomalies displayed in Fig. 9 was that this value should be about half the maximum occurring in either time series. Thus values of |0.75| and |1.5| were used for the simulation and observations respectively. For La Niña events, the negative SST anomalies in Fig. 9, the frequency of occurrence of these events is quite different between the first 200 years and years 560 to 770. There is another quiescent period between years 400 and 560. Examination of the actual SST anomaly patterns clearly shows the varying intensity of the La Niña events during these periods and confirms the change in their secular characteristics. The El Niño events in Fig. 9 exhibited more uniformity in their occurrence, but a noticeable quiescent period can be seen between about 700 and 800 years.

A preliminary analysis of a 10,000-year simulation made with the same CSIRO GCM exhibited even more marked secular variability. For example, a 1500-year period without any La Niña events with SST magnitudes above |0.75 K| occurred, while individual millennia for El Niño events showed fourfold variations in the frequency of such SST amplitudes.

While the observations in Fig. 9 are of very limited duration there is a suggestion of long term variability in the La Niña results.

The reason for the relatively low frequency of *strong* La Niña events compared to El Niño events is that it is easier for the climatic system to 'relax', thereby producing El Niño events, rather than for it to be forced more strongly, as is required for La Niña events. For example, the latter requires a strengthening of the prevailing, low-latitude east winds, which then have to induce stronger upwelling in the eastern Pacific Ocean. Such strengthening requires sources of both energy and angular momentum. The enhanced upwelling raises the thermocline locally and brings colder water to the surface. However, the stronger mixing in the upper ocean induced by the increased wind strength acts to maintain the mixed layer depth in opposition to the enhanced upwelling. This mutual interplay acts as a natural limit on the magnitude of La Niña events. In contrast, the relaxation associated with El Niño events places minimal demands on the climate system.

What caused the secular variability so prominently displayed in these three figures? Given that no external influences were permitted in the simulation this variability is considered to be a characteristic of natural climatic variability (see Hunt 1998, 2000b, 2001; Hunt and Elliott 2002) for other examples of this phenomenon), *with stochastic processes being the intrinsic generator of decadal and longer responses*. Such processes would then be responsible, for example, for the quiescent period in the observed SOI between 1920 and 1940 (Allan et al. 1996). This does not preclude a role of deterministic influences in the climatic system as complex, long-lasting atmospheric–oceanic interactions obviously occur. ENSO events are the most obvious example of such interactions. Nevertheless, the *causes* of the differences between ENSO events, and they are all unique, and their decadal variability, are attributable to stochastic influences. Graham (1994) and Barnett et al. (1999) give examples where deterministically forced coupled modes may be associated with *decadal* variability, but the latter specifically invoke a role for stochastic processes in their proposed mechanism.

An example of the *impact* of the secular variability of the simulated ENSO events is given in Fig. 10. This compares time series of the annual mean SOI and annual mean rainfall anomalies (for a small equatorial Pacific region, 2.5°S to 2.5°N, 180° to 200°E) after smoothing

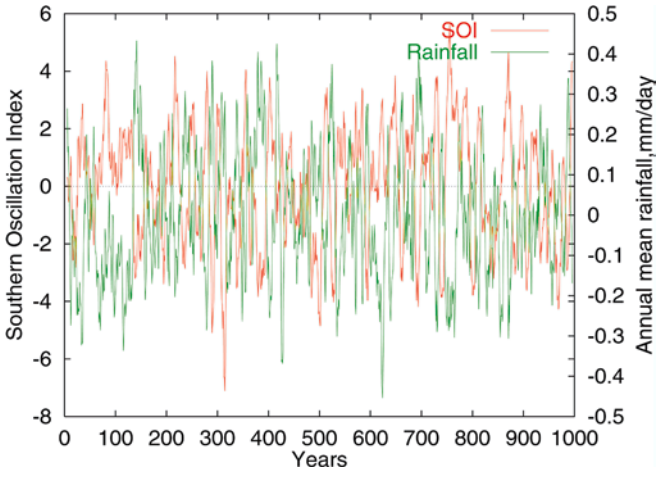

Fig. 10 Time series of annual means of the SOI and rainfall for a small Equatorial region (2.5°S to 2.5°N, 180° to 200°E) after smoothing with a 10-year running mean

with a 10-year running mean. This time smoothing highlights the decadal and longer term temporal variability. The two time series are correlated at the level of –0.56, significant at the 99.9% level. Secular influences can be seen in the figure, despite the stationarity of the simulated climate, especially in the first 150 years where a long duration dry episode occurred. The abrupt, simultaneous transitions in sign for both the time series associated with the termination of the major oscillations are particularly impressive.

Based on the time-series in Fig. 10 time-averaged climatic states were examined for the anomalous period 80 to 120 years. These revealed an overall La Niña event prevailed, although the magnitude was very small (∼0.2 K) as individual El Niño and La Niña events tend to cancel out when time averaged. Nevertheless, a distinct negative rainfall anomaly (∼0.3 mm/d) occurred over the Pacific Ocean, starting at the equatorial dateline and oriented northwest/southeast. The characteristic horseshoe of opposite signed rainfall anomalies was located westwards. Noticeable positive and negative rainfall anomalies occurred over Central America and India respectively. Finally, a low-level, easterly wind anomaly extended over much of the western and central Pacific Ocean, consistent with the prevailing La Niña conditions. Thus, the SOI time series in Fig. 10 can be readily used to identify secular variability of ENSO-forced climatic impacts.

In summary, while the simulated SOI indicates a stationary climatic state was generated by the model, secular variability could be readily identified within the time series. This manifested itself in terms of periods of low activity and decadal length trends, as well as a marked asymmetry in the occurrence of strong El Niño as opposed to La Niña events. Given the lack of any time-varying external forcing in the model, then stochastic processes are presumably the cause of such secular variability.

3.2 Persistent ENSO sequences

While persistent ENSO sequences are not unusual in the historical record (Allan and D'Arrigo 1999), the extensive El Niño event of the 1990s resulted in claims (Trenberth and Hoar 1996) and counter claims (Harrison and Larkin 1997; Rajagopalan et al. 1997) concerning the possibility of a greenhouse influence on this particular event. A discussion on the occurrence of *strong* ENSO events was presented already; here the emphasis is on *persistence* of ENSO events. The definition of a persistent event can be rather arbitrary, but here it is taken to be an event, El Niño or La Niña, with a duration of at least four years, during which time the monthly mean NINO3.4 surface temperature anomaly did not change sign. In contrast, the SOI value, which tends to have more temporal variability, was permitted to change sign during such a sequence, while having a sign predominantly associated with the event identified by the temperature anomaly, i.e. El Niño or La Niña. The amplitude of the NINO3.4 anomaly also has to be considered in determining whether an event is considered to persist.

Figure 11 illustrates two well-defined, persistent ENSO events. The El Niño event centred on year 312, Fig. 11a, had a particularly large maximum value for the SOI. Most other persistent El Niño events have SOI values peaking around –20. This event had a duration of five years, with well-sustained temperature anomalies in the NINO3.4 region. This particular event can also be identified in Figs. 8 and 9. The La Niña event centred on year 277, Fig. 11b, had a duration of six years, but a less dominant SOI signal compared to Fig. 11a.

The various persistent ENSO events identified in the 1000-year simulation are documented in Table 1. Six El Niño and nine La Niña events were identified using these defined criteria. Using a different definition based on the December to February SOI value, Allan and D'Arrigo (1999) reported 15 persistent ENSO events (having a duration of four years or longer), for the approximate 300-year period from 1706–1994. The same definition was not used to estimate the simulated long duration ENSO events, as the smallness of the temperature anomalies in the model resulted in rather noisy pressure perturbations, as can be seen in Fig. 11. Both the simulated and observed results suggest that return periods greater than 1,000 years for persistent (five years or longer) ENSO events, estimated by Trenberth and Hoar (1996) using a statistical model, are not appropriate.

A fundamental question is what causes persistent ENSO sequences? Typical observations in the NOAA Climate Diagnostic Bulletin show that ENSO events occur when large coherent oceanic temperature anomalies in the mixed layer ocean of the equatorial Pacific Ocean penetrate to the surface in the eastern Pacific Ocean, after traversing from the west. Examination of all 1000 years of annual mean outputs from the model, using a film loop, revealed that every ENSO event, even relatively minor and short duration (1 year) cases, was

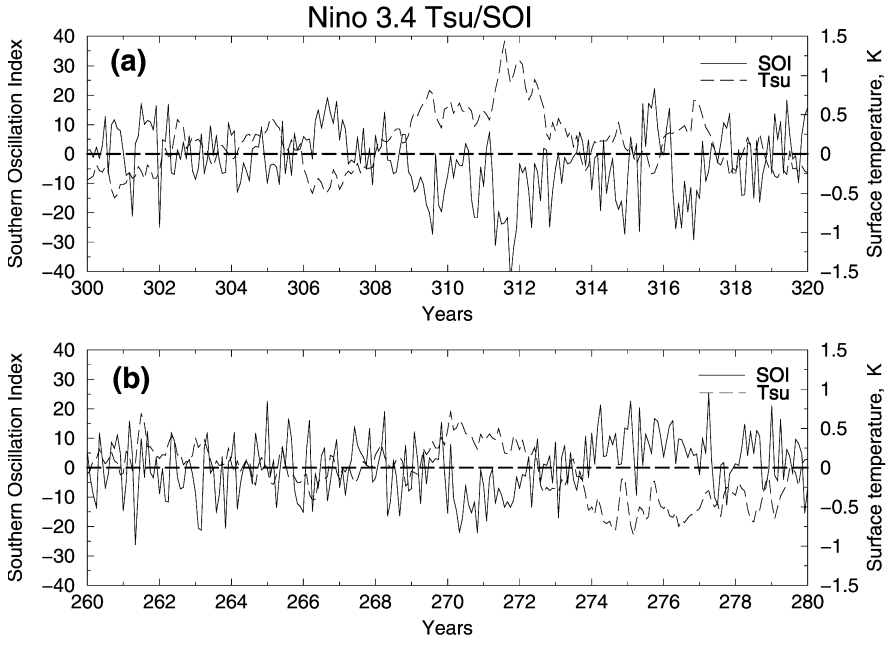

Fig. 11a, b Persistent ENSO events in the 1000-year simulation. *Top*, El Niño event, *bottom*, La Niña event. Monthly values are shown in the figure for the SOI and NINO3.4 sea surface temperature

Table 1 Persistent ENSO events, years of occurrence

El Niño	La Niña
309–314	199–205
485–489	248–253
502–506	274–280
589–596	355–360
688–695	398–403
879–884	421–426
	726–732
	810–814
	993–999

associated with such a process. The peak temperature anomalies were usually located at a depth of 50 to 100 m, having initially developed at a depth of 100 to 200 m in the western Pacific Ocean. These anomalies are simply a reflection of the change in the orientation of the local isotherms associated with the response of the thermocline to the surface wind stresses. On numerous occasions substantial, well-defined anomalies did not penetrate to the surface and ENSO events did not then occur. An understanding of the mechanisms involved in determining when, or whether, a given anomaly penetrates to the surface would greatly enhance knowledge of the processes involved in creating ENSO events. An example of such oceanic temperature anomalies, which occurred in conjunction with the extended El Niño event in Fig. 11a, is shown in Fig. 12 for years 309 to 314. As can be seen a persistent oceanic temperature anomaly was an intrinsic component of this event, with the anomaly extending from depth to the surface, although the maximum value was normally at about 50 m depth. Examination of monthly values corresponding to the annual mean time series in Fig. 12, revealed high consistency in the month-to-month pattern of positive anomalies. Even late in year 310 when this anomaly became somewhat weaker, it subsequently re-established itself in situ, as opposed to being replaced by a new anomaly transiting from the west. Much more variability was apparent in the negative temperature anomalies in the west Pacific Ocean mixed layer. However, starting late in year 311, they strengthened and eventually dominated the positive anomalies by the end of year 313. Thus, a prerequisite for a persistent El Niño event is the multi-annual residence of an oceanic temperature anomaly in the mixed layer of the central and eastern Pacific Ocean, as opposed to a succession of transient positive anomalies emanating from the western Pacific Ocean. The limited observations to date in the NOAA Climate Diagnostics Bulletin appear to support this scenario. The major difference between the observations and the current simulation is that the former have much larger amplitude temperature anomalies, a result consistent with the model's underestimation of ENSO SST anomalies.

Time series of these mixed layer temperature anomalies and low level, zonal wind anomalies over the tropical, west central Pacific Ocean, Fig. 13, were correlated at the 0.50 level for zero lag, and at –0.23 with the ocean lagging by one year. These time series illustrate that the influence of the wind anomalies extends deep into the mixed layer.

For the annual mean conditions shown in Fig. 13 it can be seen that extended El Niño events are associated with corresponding long lasting westerly wind anomalies. This relationship holds up generally when monthly wind anomalies are examined. In the case of La Niña events the correspondence between the two time series in Fig. 13 is somewhat weaker. For the time-frame shown in Fig. 12 the coherence between the two time series in Fig. 13 is particularly clearly displayed.

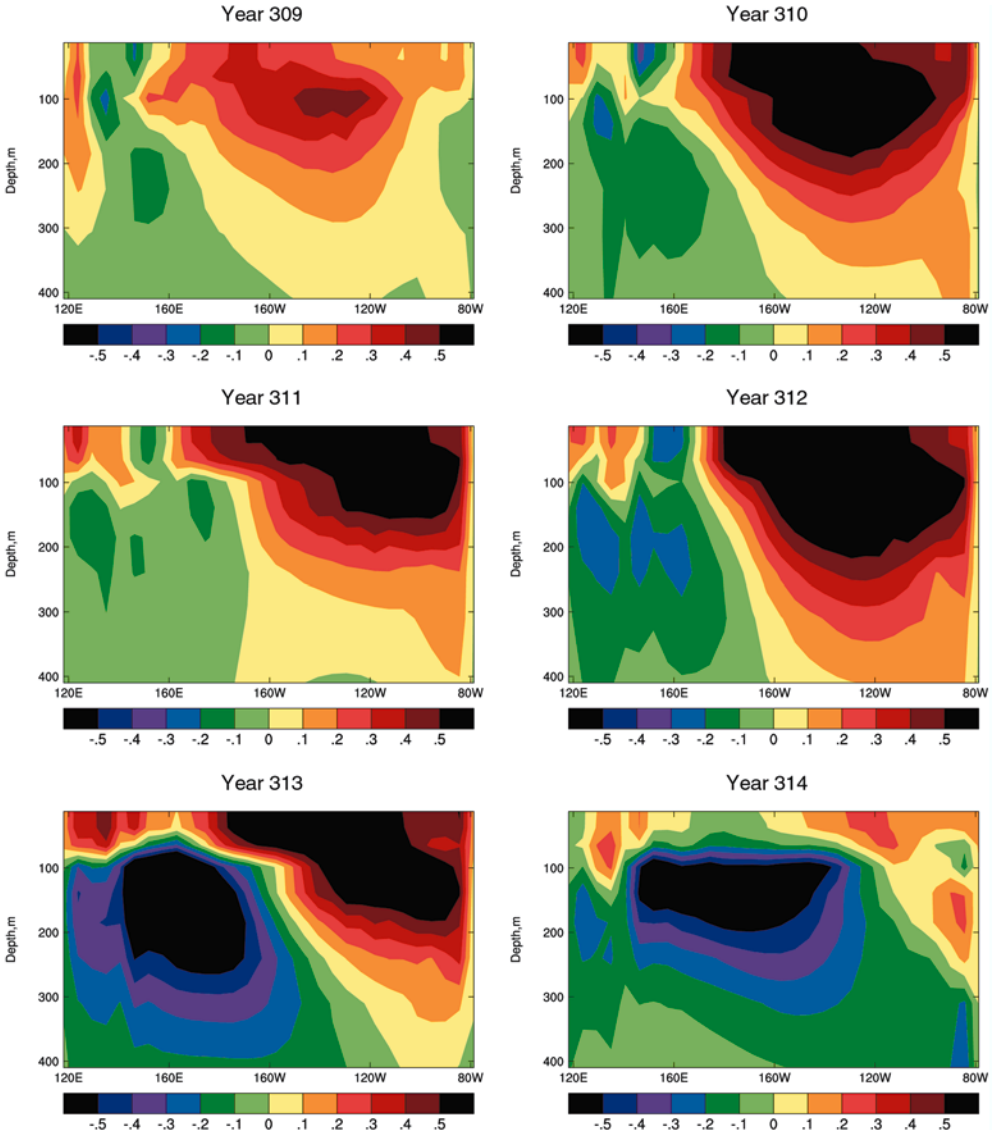

Fig. 12 Annual mean oceanic temperature anomalies for an equatorial section of the Pacific Ocean for years 309 to 314 of the simulation, which correspond to the persistent El Niño event in Fig. 11. The *colour bar* is in degrees C

Fedorov (2002) suggests, on the basis of experiments with a highly simplified coupled model, that persistent El Niño events are generated when a westerly wind burst occurs over the Pacific Ocean late in the time cycle of an existing El Niño event. The present simulation indicates that continuous (essentially at the monthly level) westerly wind anomalies are required rather than a single, isolated event.

However, it remains unclear how such persistent sustaining *wind* anomalies are maintained.

In an analysis of the extended 1991 to 1993 ENSO event, Boulanger and Menkes (1995) concluded that wind forcing over the western Pacific Ocean rather than the vagaries of western boundary reflection of oceanic Rossby waves was responsible for generating the Kelvin waves associated with the extension of this event. They acknowledged that this is not a universally accepted view.

Examination of model time series for NINO3.4 surface temperature anomalies and low-level zonal wind anomalies over the *western* Pacific Ocean (6°S to 6°N, 160°E to 180°E), for the extended ENSO event in Fig. 12 as well as short-lived events, failed to support this hypothesis. In the case of the El Niño event in Fig. 12, the largest westerly wind anomaly occurred during the dying phase of this event. In fact, the event commenced when weak easterly wind anomalies occurred in the time series mentioned.

The previous discussion highlights the mutual interaction between low-level, west winds and the occurrence of persistent ENSO events. As such, this represents a typical climatic conundrum: namely, a consistent relationship can be identified between climatic variables for a given phenomenon, without any clear identification of a precursor term. It is possible to surmise a range of causative processes, including a reflection of oceanic waves at the meridional boundaries, long duration oceanic perturbations, anomalous processes in the mixed layer ocean, etc. However, given the relative frequency of persistent ENSO events, see Allan and D'Arrigo

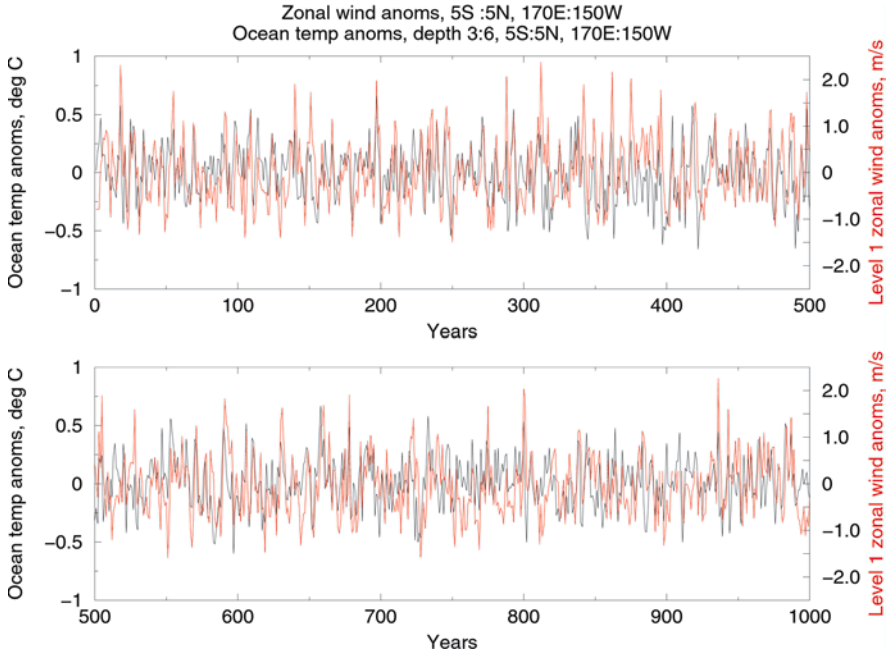

Fig. 13 Time series of annual mean low level zonal wind anomalies (983 mb) for the region 5°S to 5°N, 170°E to 150°W, and oceanic temperature anomalies for the region 5°S to 5°N, 170°E to 150°W mass weighted for model levels 3 to 6 (65 m to 185 m)

(1999) and Table 1, a simpler explanation is that stochastic processes are such that occasionally they just cause an existing ENSO event to persist.

3.3 Characteristics of the depth of the 20 °C isotherm

Hovmoeller diagrams of the depth of the 20 °C isotherm in the tropical Pacific Ocean are a regular feature of the NOAA Climate Diagnostics Bulletin, where they are used primarily to illustrate perturbations associated with ENSO events. During a typical El Niño event, for example, this isotherm shoals in the west Pacific Ocean, and deepens in the east, following the changes in intensity of the surface tropical zonal wind. A relatively short observational record exists and it is therefore of value to identify the range of variability simulated in the present 1000-year model run.

Hovmoeller diagrams of the depth of the 20 °C isotherm in the tropical Pacific Ocean were produced for the simulation by averaging between 5°S to 5°N, as were anomalies from the 1000-year mean. For brevity only anomalies will be presented here. (The total fields exhibited a similar range of depths as for the observed 20 °C isotherm, while their temporal evolution was also similar to observations). The Hovmoeller diagram of the anomalies was viewed via a film loop. This revealed numerous occasions where shoalling or deepening of the 20 °C isotherm occurred in response to ENSO events, with a clear progression of anomalies from west to east, as observed. There were also frequent periods where the anomalies showed little or no phase progression, with the characteristic features then being seasonal and interannual changes. These periods were usually associated with weak (± 0.25 °C) temperature anomalies in the tropical Pacific region or following the termination of a strong ENSO event. Typical examples are illustrated in Fig. 14 where the deepening of the depth of the 20 °C isotherm in the west and the subsequent phase progression to the central Pacific, centred on about year 150 (left hand panel), was associated with an El Niño event that peaked late in year 151, see Fig. 13. Increasingly strong westerly wind anomalies over the west and central Pacific Ocean were identified with the phase progression shown in this panel. The shoalling of the 20 °C isotherm depth in Fig. 14 (right hand panel), where little phase progression is apparent, occurred following a major El Niño event terminating in year 313, see Fig. 11 and Fig. 12. This was followed by a period with weak (± 0.25 °C) temperature anomalies in the tropical Pacific Ocean, see Fig. 11, indicating minimal ENSO activity. The zonal wind anomalies during this period were also weak, Fig. 13, hence there was little forcing of mixed layer temperature anomalies, and no reason for a corresponding phase progression of the 20 °C isotherm depth, as confirmed in the right panel of Fig. 14. A situation somewhat similar to that displayed in this panel, though of shorter duration, is apparent in the NOAA Climate Diagnostic Bulletin for the period 1999 to 2001, during which a weak La Niña event has prevailed. The mixed layer temperature anomalies, discussed in relation to Fig. 12, tend to be centred along the depth of the 20 °C isotherm. This is more clearly apparent in the *monthly* datasets in the NOAA Climate Diagnostic Bulletin. It is then these anomalies which are responsible for the consequent changes in the height of this isotherm, which in turn derive from the surface wind forcing shown in Fig. 13.

To investigate the secular variability of this isotherm depth a temporal index was created by averaging the depth of the anomalies over the region 5°S to 5°N and 140°E to 80°W, essentially the width of the tropical

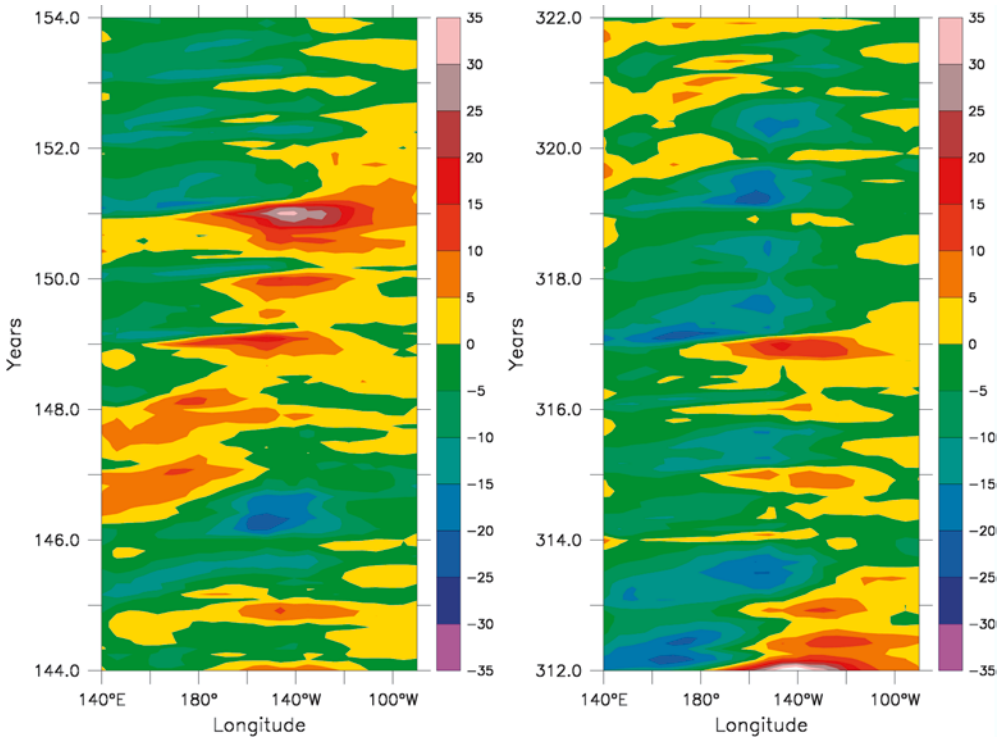

Fig. 14 Anomalies of the depth of the 20 °C isotherm across the equatorial Pacific Ocean averaged between 5°S to 5°N for two selected time periods in the 1000-year simulation. The *colour bar* gives the change in depth of the anomalies in metres

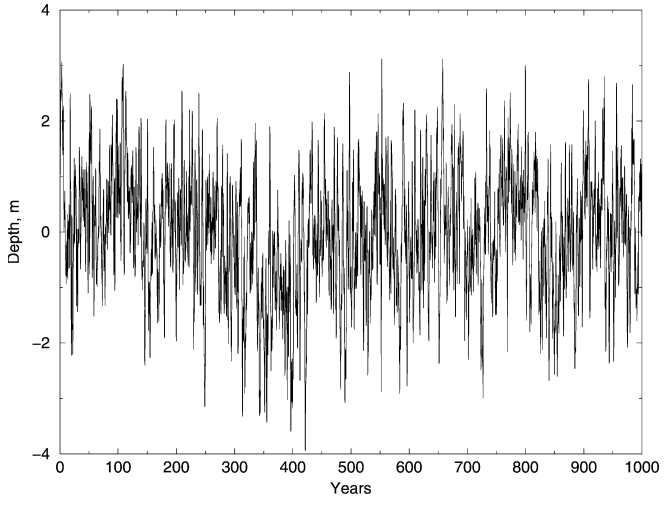

Fig. 15 Index of temporal variability of anomalies in the depth of the 20 °C isotherm based on an average from 5°S to 5°N and 140° to 180°E

Pacific Ocean. The time-smoothed version of this index is presented in Fig. 15, where noticeable secular variability can be identified, in particular centred near years 350 and 850 years. A particularly strong series of La Niña events occurred between years 350 to 360, while extensive La Niña events of various intensities prevailed between years 810 to 900, as can be partially identified in Fig. 13. These events were associated with easterly wind anomalies, enhanced depths of the 20 °C isotherm in the west Pacific Ocean, and weaker oceanic currents. Apart from this secular variability the index is characterised by interannual (i.e. ENSO) perturbations.

In the unsmoothed time series corresponding to Fig. 15 there were extreme outliers with very negative depths on five or six occasions. All these outliers were associated with La Niña events of varying intensities, as judged by surface temperature anomalies. Such outliers are an indicator of stochastic influences and presumably are indicative of related stochastic responses resulting in secular variability. These results suggest that observations to date have only sampled a limited range of the possible variability of the 20 °C isotherm.

Two practical points arise from Figs. 14 and 15. The first concerns the identification of episodes such as that shown in the right hand panel of Fig. 14. Given the weak SST anomalies associated with such episodes this portends a period of low climatic variability and predictability. The second point represents the reverse situation when secular variability, as shown in Fig. 15, suggests the occurrence of enhanced La Niña events could be expected. This would be a time of marked climatic variability and enhanced predictability. The possibility exists that such episodes may be predictable.

In particular, monitoring of anomalies in the 20 °C isotherm in prediction experiments, as displayed in Fig. 14, could be a useful tool for assessing not only the performance of the model, but also the ensuing development of ENSO events.

3.4 PNA response

The Pacific North America (PNA) oscillation is recognised as an important climatic link between the equatorial Pacific Ocean and the Northern Hemisphere

(Horel and Wallace 1981). Part of the excitation of this oscillation appears to be generated by stochastic processes intrinsic to the atmosphere according to simulations by Lau (1997). Also Rodionov and Assel (2001) found two PNA characteristics which were associated with SST variability in the *north* Pacific Ocean and ENSO events respectively. These results imply that the schematic PNA pattern of Horel and Wallace (1981), which they attributed to warm SST conditions in the equatorial Pacific Ocean, is not necessarily a robust feature of the climatic system. Thus the question arises as to whether secular variability of ENSO can excite secular variability of the PNA oscillation.

To investigate this possibility the PNA oscillation simulated in the 1000-year experiment was examined in some detail. This oscillation was defined as the anomaly of the 200 mb geopotential height (Z200) for a given month from the corresponding 1000-year mean for that month, averaged over December, January and February. An EOF analysis was made of the 1000-year Z200 oscillations.

Figure 16 compares EOF1 and EOF2 spatial patterns and their related time series, after the latter have been smoothed with a 10-point running mean. EOF1 replicates some of the characteristics of the idealised PNA pattern of Horel and Wallace (1981), but overall the pattern is too zonal. The variance explained by EOF1 is 12.4%. The EOF2 pattern is closer to the idealised PNA, particularly over North America, but, as depicted, has the opposite phase. Subsequent analysis is therefore based on EOF2. The variance explained by EOF2 is 9.2%. EOF3 and EOF4 explained 7.8% and 6.5% of the variance respectively, but had little resemblance to the EOF1 and EOF2 patterns. The relatively small amount of variance identifiable with the intrinsic PNA patterns demonstrates why this pattern can be difficult to identify on occasions when viewing the original Z200 oscillations.

The time-smoothed time series in Fig. 16c and d, corresponding to EOF1 and EOF2 respectively, reveal decadal and multi-decadal variability. Correlation of these time series with similarly time-smoothed NINO3.4 surface temperature anomalies produced correlation coefficients of –0.48 and –0.23 respectively, which are significant at the 99% level given the 1000-year duration of the data. These correlations indicate that a component of the PNA decadal signal is attributable to ENSO forcing.

The PNA response to the secular variability of ENSO was investigated for two episodes identified in the EOF2 time series in Fig. 16d, specifically for years 180 to 210 and 840 and 890. These represent different phases of the PNA. The composited original PNA patterns for these episodes are shown in Fig. 17. The PNA pattern for the positive phase, Fig. 17a, reproduces the idealised figure of Horel and Wallace (1981) extremely well. That for the negative phase, Fig. 17b, is somewhat less well-structured. Given the high frequency variability of the

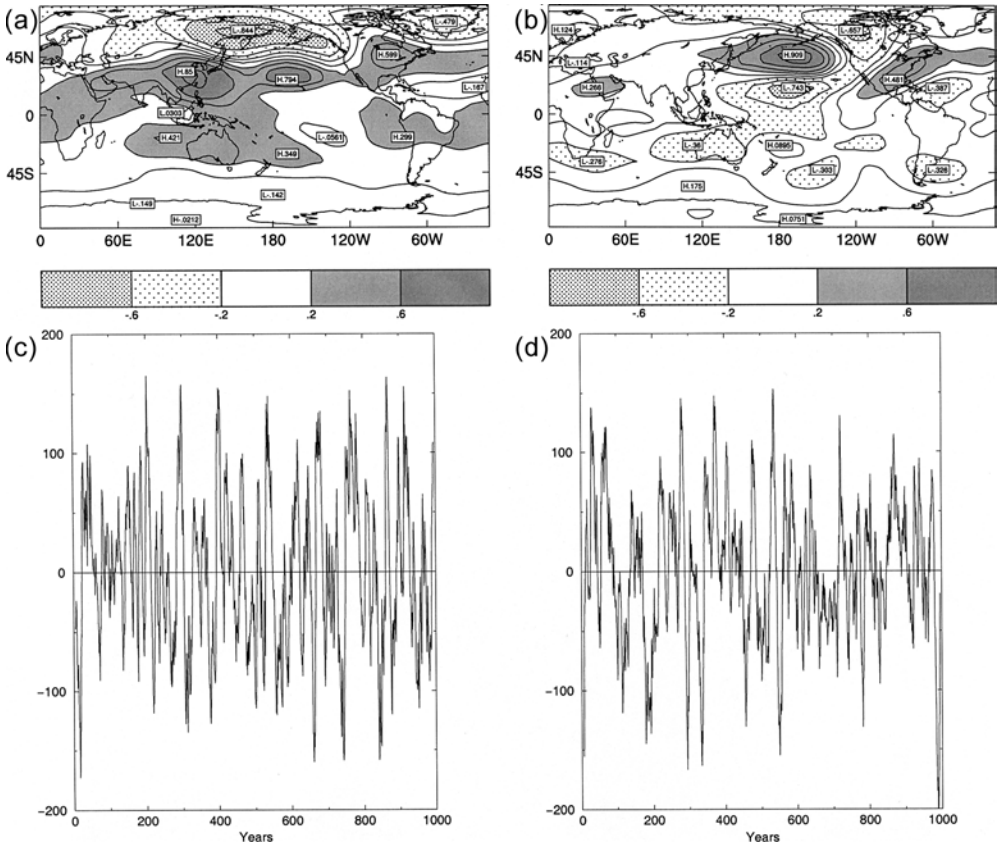

Fig. 16a–d Spatial patterns of the Z200 geopotential height for December, January and February mean conditions, **a**, EOF1; **b**, EOF2. The *lower panels* contain the respective time series which have been smoothed with a 10-point running mean filter

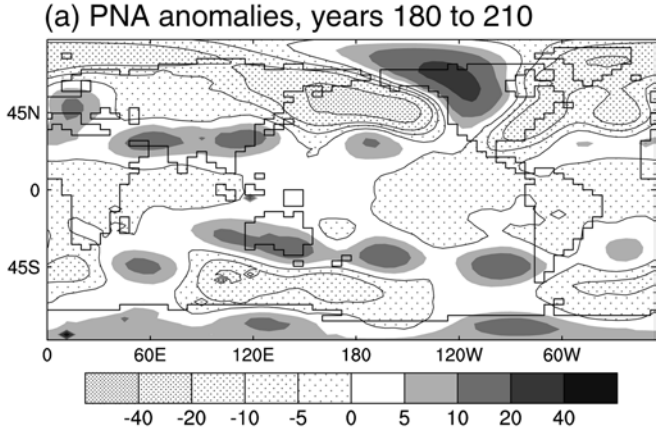

Fig. 17a, b Composited PNA anomaly patterns for two specified periods for December, January and February mean conditions

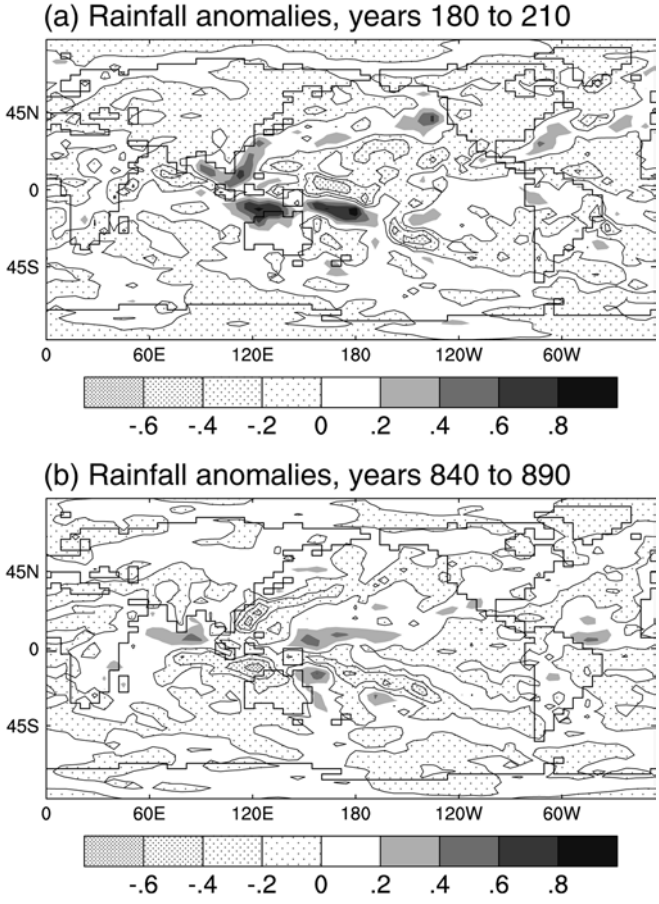

Fig. 18a, b Composited rainfall anomaly patterns for the same two specified periods as used in Figure 17 and for December, January and February mean conditions

unsmoothed time series associated with EOF1 and EOF2 patterns (not shown), the results in Fig. 17 reveal surprisingly stable underlying PNA oscillations during these episodes.

As shown in Fig. 18, distinct, but small, rainfall anomalies were associated with these two episodes. Over North America, where a PNA response is to be expected, continent-wide rainfall anomalies of opposite signs occurred. Interestingly, similar types of responses can be seen in Fig. 18 over Australia, Indonesia and the Philippines. The latter are presumably directly related to the normal ENSO forcing in this region rather than having a PNA connection. Although not shown here, related impacts were obtained for surface temperature anomalies over North America.

The two episodes considered here were primarily, but not exclusively, associated with El Niño events (years 180 to 210) or La Niña events (years 840 to 890). This indicates that despite the influence of stochastic processes on the PNA oscillation (Lau 1997), for appropriate time-averaged situations there can be a discernible climatic impact over Northern America. Importantly, the current simulation identifies the existence of distinct PNA impacts associated with secular variability of ENSO events.

The sensitivity of the PNA oscillation to tropospheric wind shear (Lau 1997) was evaluated by calculating the vertical shear of the zonal wind between approximately 3 and 11 km for all 1000 years of the simulation for a box over the North Pacific Ocean (30° to 40°N, 180°E to 200°E). The correlation of this time series to the EOF1 and EOF2 time series in Fig. 16 was –0.02 and –0.78 respectively. As noted EOF2 was considered to be more representative of the PNA oscillation. The EOF2 correlation implies that large amplitude PNA oscillations correspond to low vertical shear of the zonal wind. Thus a component of the secular variability of EOF2 evident in Fig. 16d can be related to atmospheric variability associated with changes in wind shear.

3.5 Skewness and kurtosis

Some useful insight into temporal variability of a given climatic time series is provided by calculating its skewness and kurtosis (Burgers and Stephenson 1999). Here skewness is defined as $\sqrt{b_1} = m_3/m_2^{3/2}$ and kurtosis as $b_2 - 3 = m_4/m_2^2 - 3$, where $m_k = (x - \bar{x})^k$ and $\bar{x}$ is the time mean value. Following Burgers and Stephenson (1999) a reduced kurtosis is used, defined by $b_2' = b_2 - 3 - 1.5b_1$. If the values of a time series are represented by

histograms of frequency versus amplitude, then a series is said to be skewed if one of the two tails of the distribution is longer. The kurtosis of a distribution is defined to be positive if the maximum is particularly peaked, and negative if the maximum is flattened compared with the normal distribution.

As shown by Burgers and Stephenson (1999) these statistical measures provide a useful means of identifying individual ENSO regimes sampled in the 1000-year simulation. Thus in Fig. 19 such statistics are plotted for NINO3 SST anomalies as consecutive 50-year samples taken from the 1000-year output.

The NINO3 region is used in Fig. 19 to permit a direct comparison with the observational results (for 1950–1997), taken from Table 2 of Burgers and Stephenson (1999), as indicated by the cross in this figure. The model results reveal that a range of climatic conditions were sampled in the simulation, but with an overall positive skewness. Most model samples were well removed from the observed value, raising interesting questions concerning how much variability might be expected in a more extended observational record.

Burgers and Stephenson (1999) presented results similar to Fig. 19 for three other models, all of which produced quite different behaviours to the current model. One, a simple one-variable conceptual model, had outputs only in the bottom, left hand quadrant; the intermediate Cane-Zebiak coupled model had outputs in all quadrants, while the NCAR CSM (a coupled GCM similar to the present model) had outputs clustered around the origin of the figure. Thus, the formalism represented by Fig. 19 *might serve as a useful test of coupled model behaviour*. Presumably, a model generating an appropriate range of internal climatic variability should be expected to sample a wide range of ENSO states, as indicated in Fig. 19.

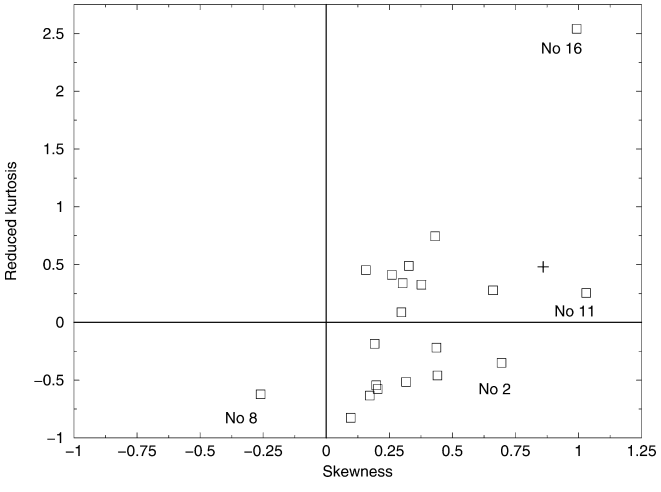

Fig. 19 Skewness-reduced kurtosis diagram of NIÑO3 surface temperature anomalies from the 1000-year simulation. The model output was analysed in twenty 50-year blocks. The *numbered blocks* in the diagram are according to their ranking in the twenty block total and are referred to individually later. The *cross* in the figure defines the observed value for the period 1950 to 1977

Histograms of frequency of occurrence versus amplitude of the NINO3 monthly mean screen temperature anomaly were examined for the four 50-year time blocks identified in Fig. 19. While such time blocks are relatively short from a statistical viewpoint, it is the climatic variability associated with such periods which is of interest in a secular investigation. For example, a quite different histogram was obtained for block 8 compared to the other three blocks, suggesting that this is a useful tool in identifying secular variability.

4 Conclusions

An analysis has been made of a number of aspects of ENSO variability derived from a 1000-year simulation with the CSIRO Mark 2 coupled global climatic model. In common with most other current models, the present model underestimates the magnitude of the observed SST anomalies associated with ENSO events, but replicates many of the critical features associated with ENSO-induced climatic variability. This is demonstrated by systematic comparisons with outputs from the NCEP/NCAR reanalysis data set.

The 1000-year time series of the simulated SOI suggests that ENSO is a very robust feature of present climate. Such stability does not preclude secular variability, as the SOI was shown to have a range of perturbations, with noticeable secular responses associated with the occurrence of strong El Niño and La Niña events. Persistent ENSO events were found to be a natural outcome of the simulation, indicating that the observed, extended El Niño of the 1990s was not exceptional. The simulation highlighted the role of the mixed layer ocean temperature anomalies in the development of ENSO events, and a better appreciation of the dynamics of such anomalies is clearly desirable.

While ENSO events are characterised by deterministic coupled atmospheric-oceanic modes, and such modes also appear to contribute to decadal variability, it is concluded that stochastic processes are the primary driver for the climatic variability displayed in the model. This conclusion would appear to be firmly based given the exclusion of all external forcing mechanisms from the simulation. Even if eventually it can be shown that deterministic coupled modes govern some observed decadal variability, the intra- and inter-decadal variability associated with such modes would still indicate the importance of stochastic processes.

The output from the simulation suggest that one aspect of ENSO variability, namely the evolution of anomalous height of the 20 °C isotherm in the ocean, may exhibit a large range of activity than has been observed to date. The routine monitoring of such anomalies in multi-seasonal predictions may provide a guide to possible outcomes.

The model simulated the behaviour of the PNA oscillation surprisingly well, and the analysis indicates that ENSO events are an important forcing mechanism in

such oscillations. Certainly, secular variability of ENSO-related PNA patterns and impacts over North America were obtained in the simulation. This secular aspect of North American climate would appear to be worth examining in more detail.

Finally, as shown by this and other analyses of millennial-scale simulations, a very rich resource exists for future exploitation as regards our understanding of climatic processes.

Acknowledgements The authors thank Dr A.C. Hirst for making available the output of the 1000-year simulation.

References

AchutaRao K, Sperber KR (2000) El Niño Southern Oscillation in coupled models. PCMDI Rep 61, PCDMI, Lawrence Livermore National Laboratory, Livermore 95440, USA

Allan RJ (2000) ENSO and climatic variability in the last 150 years. In: Diaz HF, Markgraf V (eds) El Niño and the Southern Oscillation: multiscale variability, global regional impacts. Cambridge University Press, Cambridge, UK (in press) ch 1

Allan RJ, D'Arrigo RD (1999) 'Persistent' ENSO sequences: how unusual was the 1990–1995 El Niño. The Holocene 9: 101–118

Allan RJ, Lindesay JA, Parker DE (1996) El Niño Southern oscillation and climate variability. Melbourne, CSIRO Publishing, pp 405

Barnett TP, Pierce DW, Latif M, Dommenget D (1999) Interdecadal interactions between the tropics and midlatitudes in the Pacific basin. Geophys Res Lett 26: 615–618

Boulanger J-P, Menkes C (1995) Propagation and reflection of long equatorial waves in the Pacific Ocean during the 1992–1993 El Niño. J Geophys Res 100/C12: 25,041–25,059

Burgers G, Stephenson DB (1999) The "normality" of El Niño. Geophys Res Lett 26: 1027–1030

Chao Y, Ghil M, McWilliams JC (2000) Pacific interdecadal variability in this century's sea surface temperatures. Geophys Res Lett 27: 2261–2264

Covey C, AchutaRao KM, Lambert SJ, Taylor KE (2000) Intercomparison of present and future climates simulated by coupled ocean–atmosphere GCMs. PCMDI Rep 66, PCDMI, Lawrence Livermore National Laboratory, Livermore 94550, USA

Diaz HF, Markgraf V (eds) (1992) El Niño: historical and paleoclimatic aspects of the Southern Oscillation. Cambridge University Press, Cambridge, England, pp 476

Diaz HF, Pulwarty RS (1994) An analysis of the time scales of variability in centuries-long ENSO-sensitive records in the last 1000 years. Clim Change 26: 317–342

Fedorov AV (2002) The response of the coupled ocean–atmosphere to westerly wind bursts. Q J R Meteorol Soc 128: 1–23

Gordon HB, O'Farrell SP (1997) Transient climate change in the CSIRO coupled model with dynamical sea ice. Mon Weather Rev 125: 875–907

Graham NE (1994) Decadal-scale climate variability in the 1970s and 1980s: observations and model results. Clim Dyn 10: 135–159

Harrison DE, Larkin NK (1997) Darwin sea level pressure, 1876–1996: evidence for climate change? Geophys Res Lett 24: 1779–1782

Hirst AC, O'Farrell SP, Gordon HB (2000) Comparison of a coupled ocean–atmosphere model with and without eddy-induced advection. 1. Ocean spin-up and control integrations. J Clim 13: 139–163

Horel JD, Wallace JM (1981) Planetary-scale atmospheric phenomena associated with the Southern Oscillation. Mon Weather Rev 109: 813–829

Hunt BG (1998) Natural climatic variability as an explanation for historical climatic fluctuations. Clim Change 38: 133–157

Hunt BG (2000a) Multiseasonal hindcasts for 1972–1992. Mon Weather Rev 128: 1474–1489

Hunt BG (2000b) Natural climatic variability and Sahelian rainfall trends. Glob Plan Change 24: 107–131

Hunt BG (2001) A description of persistent climatic anomalies in a 1000-year climatic model simulation. Clim Dyn 17: 717–733

Hunt BG, Elliott TI (2002) Mexican megadrought. Clim Dyn 20:1–12

Knutson TR, Manabe S (1994) Impact of increased CO_2 on simulated ENSO-like phenomena. Geophys Res Lett 21: 2295–2298

Knutson TR, Manabe S, Gu D (1997) Simulated ENSO in a global coupled ocean–atmosphere model: multidecadal amplitude modulation and CO_2 sensitivity. J Clim 10: 138–161

Lau N-C (1997) Interactions between global SST anomalies and the midlatitude atmospheric circulation. Bull Am Meteorol Soc 78: 21–33

Lough JM (1992) An index of the Southern Oscillation reconstructed from western North American tree-ring chronologies. In: Diaz HF, Markgraf V (eds) El Niño-Historical and paleoclimatic aspects of the Southern Oscillation. Cambridge University Press, Cambridge, UK, pp 215–226

Lui Z, Huang B (2000) Cause of tropical Pacific warming trend. Geophys Res Lett 27: 1935–1938

Quinn WH, Neal VT, Antunex de Mayolo SE (1987) El Niño occurrences over the past four and a half centuries. J Geophys Res 92: 14,449–14,461

Rajagopalan B, Lall V, Cane MA (1997) Anomalous ENSO occurrences: an alternative view. J Clim 10: 2351–2357

Rodionov S, Assel R (2001) A new look at the Pacific/North American Index. Geophys Res Lett 28: 1519–1522

Timmermann A, Oberhuber J, Bacher A, Esch M, Latif M, Roeckner E (1999) Increased El Niño frequency in a climate model forced by future greenhouse warming. Nature 398: 694–697

Trenberth KE, Hoar TJ (1996) The 1990–1995 El Niño Southern Oscillation Event. Geophys Res Lett 23: 57–60

Vimont D, Battisti DS, Hirst AC (2002) Pacific interannual and interdecadal Equatorial variability in a 1000-year simulation of the CSIRO coupled general circulation model. J Clim 15:160–178

Wang XL, Ropelewski CF (1995) An assessment of ENSO-scale secular variability. J Clim 8: 1584–1599

Watterson IG, Dix MR, Gordon HB, McGregor JL (1995) The CSIRO 9-level atmospheric general circulation model and its equilibrium present and doubled CO_2 climates. Aust Meteorol Mag 44: 111–125

Wilson SG, Hunt BG (1997) Impact of greenhouse warming on El Niño/Southern Oscillation behaviour in a high resolution coupled global climatic model. Report to the Australian Department of Environment, Sport and Territories. CSIRO, Australia

Zhang X, Sheng J, Shabbar A (1998) Modes of interannual and interdecadal variability of Pacific SST. J Clim 11: 2556–2569